Plasmonic Elliptical Nanohole Array for On-Chip Human Blood Group Detection

Santosh Kumar Sahu, *Graduate Student Member, IEEE*, and Mandeep Singh, *Member, IEEE*

***Abstract*—A novel refractive index (RI) plasmonic biosensor with high sensitivity for human blood group detection is proposed and numerically investigated in the visible and near-infrared (NIR) regime. The proposed structure is based on a metal–insulator–metal (MIM) waveguide with an array of elliptical nanoholes. These nanoholes are used as the sensing surface and support important optical properties, such as extraordinary optical transmission (EOT) and nanoscale confinement of light. We have simulated and optimized the biosensor using RF module of COMSOL Multiphysics software, predicting the sensitivity values of three blood groups (A, O, and B) as 64.26, 101.16, and 82.1 nm/RIU, respectively. High sensitivity, precision, and portability make the reported sensor highly valuable for point-of-care applications, emergency situations, and resource-limited settings. By reducing the time for blood typing procedures and small sample volume requirements, MIM biosensor has the potential to enhance patient care and streamline medical processes.**

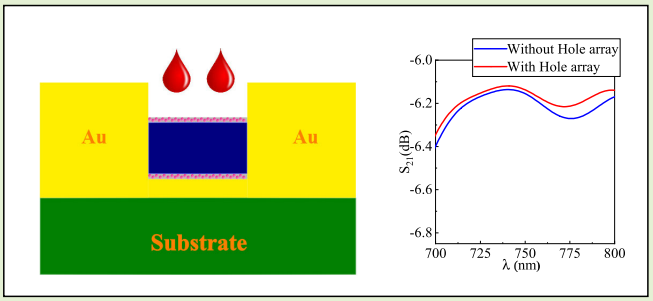

***Index Terms*— Biosensor, elliptical nanoholes, extraordinary optical transmission (EOT), metal–insulator–metal (MIM), plasmons.**

I. Introduction

IN RECENT years, the study of biosensors has increased substantially because of their significant applications in various fields, such as health care, food safety, deoxyribonucleic acid (DNA) hybridization, and many industrial applications [1], [2]. Generally, optical biosensors are classified into two categories: label-based biosensors and label-free biosensors. The binding properties of molecules change in the label-based detection technique, decreasing detection reliability. The detection of biomolecules is done directly in a label-free optical biosensor. Blood grouping is essential in blood transfusion and organ transplantation to ensure compatibility between the donor's and recipient's blood types. Traditional blood typing methods involve time-consuming manual testing procedures that may not be suitable for point-of-care or emergency conditions. On-chip blood group detection offers several advantages: speed, automation, and portability [3], [4], [5]. On-chip human blood group detection is a promising field of research with the potential to improve patient care, especially in emergency situations. Researchers and healthcare professionals continue refining these technologies to enhance their accuracy and ease of use.

The ability to manipulate the electromagnetic (EM) waves at the nanoscale level and the significant enhancement of optical effects via tight confinement in the dielectric region have made the metal–insulator–metal (MIM) structures useful for sensing applications [6]. These structures generate the SPPs with longer propagation lengths, the device's footprint is also small, the fabrication technique is quite simple, and group velocity is also high over a wide bandwidth [7]. Due to high ohmic losses, the sensitivity of the MIM structure is relatively low as compared to the classical sensors based on optical fiber [8]; hence, several efforts have been made to increase the sensitivity of these structures by coupling them with nanodisk resonators, nanorods, nanoparticles, rectangular cavity, and so on [9]. Recently, there has been a trend of utilizing nanodots and nanoholes to improve the sensitivity of cavity-based MIM sensors by enhancing light–matter interaction through the plasmon resonance condition.

Many biosensor designs have been reported using the MIM waveguide structure. Al Mahmod et al. [10] introduced a unique biosensor configuration that combines the MIM

Manuscript received 4 September 2023; revised 30 September 2023; accepted 1 October 2023. Date of publication 16 October 2023; date of current version 14 November 2023. This work was supported in part by the Department of Biotechnology, Government of India, under Project BT/PR40358/NNT/28/1756/2020, in part by the Defense Research and Development Organization under Project ERIP/ER/202202001/M/01/1793, in part by the Indian Space Research Organization under Project ISRO/RES/4/617/2021, and in part by the Council of Scientific and Industrial Research under Project 70/0083/23/EMR-II. The associate editor coordinating the review of this article and approving it for publication was Dr. Rui Min. *(Corresponding author: Mandeep Singh.)*

The authors are with the Applied Photonics Laboratory, Department of Electronics and Communication Engineering, National Institute of Technology Karnataka, Surathkal 575025, India (e-mail: mandeep.singh@nitk.edu.in).

Digital Object Identifier 10.1109/JSEN.2023.3323556

waveguide with a ring resonator structure designed specifically for biomolecular sensing applications. Maryam et al. [11] presented a label-free MIM circular plasmonic biosensor with high sensitivity, specifically designed for the detection of water impurities and DNA hybridization. Zafar et al. [12] proposed an ultracompact on-chip plasmonic sensor that utilizes the MIM waveguide structure combined with a pair of elliptical ring resonators for detecting hemoglobin concentration in blood. Sypabekova et al. [13] developed an optical-fiber biosensor that integrates a tilted fiber Bragg grating (TFBG) with a ball resonator to detect the breast cancer biomarker soluble human epidermal growth factor receptor-2 (sHER2). In their study, Melo et al. [14] developed a TFBG sensor to analyze the individual detection of several anion concentrations in ethyl acetate. More specifically, they studied the presence of acetate, fluoride, and chloride in the solution. Soares et al. [15] designed a fiber optic immunosensor using a D-shaped structure coated with a gold film. This proposed sensor specifically detects cortisol levels, serving as a stress biomarker.

The high extinction and scattering coefficients exhibited by the nanohole array present in the substrate are essential for the detection of chemical and biological elements. The surface plasmon resonance (SPR)-based sensors show favorable properties when incorporating nanohole arrays. These structures exhibit an optical response, where the transmission of light at a particular wavelength is greater than what would be predicted by classical diffraction theories [16]. This results in a higher-than-expected light intensity on the target, commonly known as extraordinary optical transmission (EOT). The EM field distribution highly depends on the geometry and orientation of the nanoholes. The elliptical nanohole array on the metal surface behaves as an intrinsically chiral lattice that will provide extremely high circular dichroism, enhancing the light–matter interaction compared to a circular hole, as discussed in [17] and [18]. In addition, by changing the thickness of the metal layer and the periodicity of the hole array, we can modify the optical properties of the sensors based on the nanohole structure, making it suitable for various research applications.

II. Modeling of Human Blood Group Biosensor

The front view of the proposed biosensor is shown in Fig. 1(a), which is a MIM structure. The substrate comprises Si material with dimensions of 300 × 1200 nm. An indirect absorption feature is used for a silicon substrate during the material assignment. The slot is chosen as SiO_2 material having a width of 250 nm and height of 50 nm. The metallic layer of various previously reported sensors, designed explicitly for THz application, generally employs gold (Au) or silver (Ag) as the active plasmonic materials. Among these two metals, Ag has a narrower resonance curve (i.e., smaller FWHM) that enhances the detection accuracy (DA) of the SPR sensors to a higher value. Still, the chemical stability of Ag is inferior. It oxidizes quickly when it comes into contact with air or any liquid, hence unsuitable for reliable sensor design. In contrast, the resonance curve of Au is broad, corresponding to any change in the refractive index

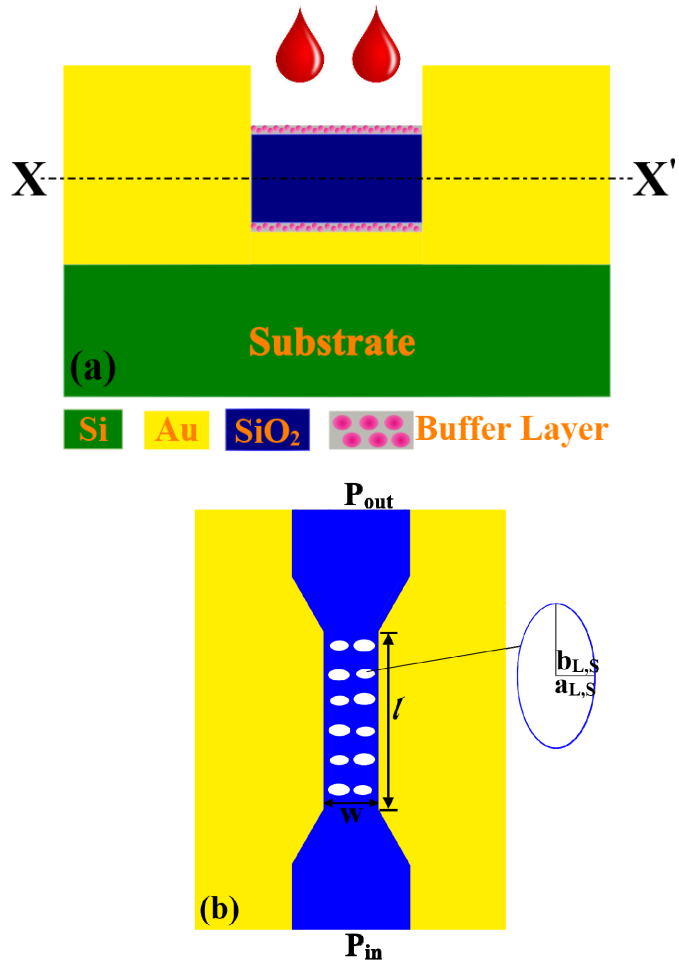

Fig. 1. (a) Front view of the proposed MIM waveguide-based human blood group biosensor. (b) Its corresponding top view. Here, "L" and "S" denote the geometric parameters for the large and small ellipse, respectively; "l" is the length of the sensing region.

(RI) of the sensing layer, and chemically more stable than Ag, which will be helpful for reliable sensor design for practical applications [19]. A thin buffer layer is added on top of the Au layer with a thickness of 1–15 nm with a constant RI of 1.45. The buffer layer acts as a biochemical layer, which avoids direct contact of the blood sample with the Au layer because it may dilute the blood sample, affecting the sensor's performance. This biochemical layer can also provide a strong bond between the blood sample and the Au layer because of its chemical and biological properties, thus preventing structural anomalies [20].

The top view of the proposed MIM sensor with a periodic array of elliptical nanoholes is illustrated in Fig. 1(b). As shown in Fig. 1(b), it is a two-port device, where P_{in} denotes the input port and P_{out} represents the output port. The sensing region's total length (l) is 1000 nm, and the width (W) is 250 nm. When the width of sensing region is exceptionally smaller than the wavelength of incident light, the coupling structure only generates the fundamental transverse magnetic (TM) mode, which can excite the surface plasmon polaritons (SPPs) [21].

Light is coupled to and from the waveguide using a tapered structure of 1000 nm length. The simulation and optimization

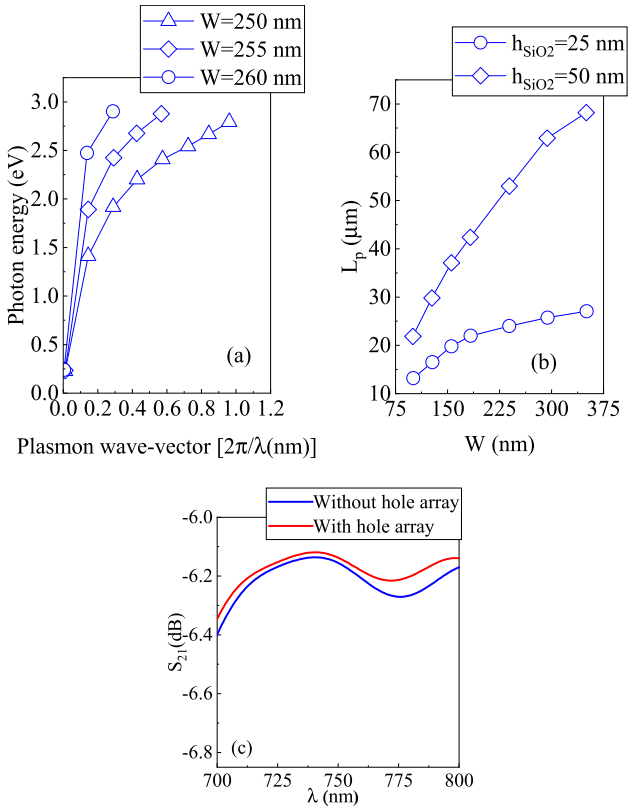

Fig. 2. (a) Dispersion plot for MIM biosensor with different insulator thicknesses (W). (b) Propagation length (L_p) versus silicon dioxide waveguide width (W). (c) Transmission plot (S_{21}, in dB) with and without nanohole array.

are carried out using the RF module of COMSOL multiphysics software [22]. The proposed sensor is discretized using a physics-controlled mesh having domain elements ∼1980 and boundary elements ∼570. The boundary condition is set to be a perfectly matched layer (PML) that will absorb the EM wave propagating outside the target area.

Generally, MIM waveguides support surface plasmon (SP) in the nanoscale with a thinner insulator layer. Fig. 2(a) depicts a dispersion relation for the proposed sensor with different insulator thicknesses. For instance, says 725 nm (1.71 eV), the SP wave vector can be varied from 0.096 to 0.228 nm by changing the insulator thickness from 260 to 250 nm. Furthermore, we have studied the dependence of propagation length [23] on the width (W) of the silicon dioxide waveguide [see Fig. 2(b)]. The transmission plot of the structure by considering both hole and without-hole cases is shown in Fig. 2(c). Fig. 2(c) shows an increase in transmission in nanostructured elliptical hole arrays, where the extraordinary optical transmission (EOT) was attributed to the tunneling via excitation of the resonant SPPs through the subwavelength structures. Creating an array of holes with the proper arrangement is possible, which provides the necessary grating momentum to generate the SPPs.

The resonant wavelength for the excitation of SPPs in a rectangular lattice structure under normal incidence is given by [24]

$$\lambda = \frac{A}{\sqrt{X^2+Y^2}}\sqrt{\frac{\varepsilon_1\varepsilon_2}{\varepsilon_1+\varepsilon_2}} \tag{1}$$

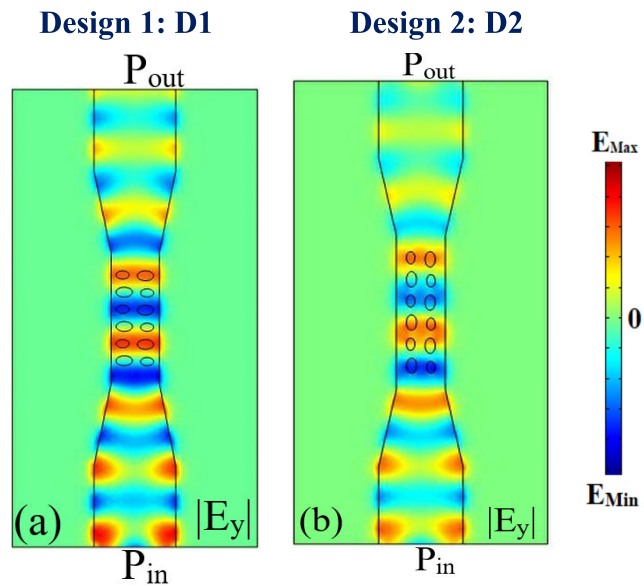

Fig. 3. Top view [slice cut along XX′ line in Fig. 1(a)] of the simulated electric field pattern (V/m). (a) Design 1 ($D1$): Horizontal orientation of elliptical nanohole array. (b) Design 2 ($D2$): Vertical orientation of elliptical nanohole array.

where A is the lattice constant, X and Y represent the mode indices numbers, ε_1 is the dielectric constant of the surrounding material, and ε_2 is the dielectric constant of the metal-like grating materials, and its value is complex.

The RI of SiO_2 depends upon the wavelength and is given by the standard Sellmeier relation as follows [25]:

$$n^2(\lambda) = 1 + \frac{C_1\lambda^2}{\lambda^2 - D_1^2} + \frac{C_2\lambda^2}{\lambda^2 - D_2^2} + \frac{C_3\lambda^2}{\lambda^2 - D_3^2} \tag{2}$$

where λ denotes the wavelength, and the Sellmeier coefficients are $C_1 = 0.696166300$, $C_2 = 0.407942600$, $C_3 = 0.897479400$, $D_1 = 0.0684043$, $D_2 = 0.1162414$, and $D_3 = 9.896161$, respectively. The Drude model is employed to calculate the complex permittivity of the metal (Au) layer [23] and is given by the following relation:

$$\begin{aligned}\varepsilon_{\text{metal}}(\lambda) &= \text{Re}(\varepsilon_{\text{metal}}) + \text{Im}(\varepsilon_{\text{metal}}) \\ &= 1 - \frac{\lambda^2\lambda_C}{\lambda_P^2(\lambda_C + i\lambda)}\end{aligned} \tag{3}$$

where λ_P(168.26 nm) denotes the plasma wavelength and λ_C (8934.2 nm) denotes the collision wavelength for gold.

The top view of the simulated tangential electric field (E_y) of design 1 ($D1$) and design 2 ($D2$) are shown in Fig. 3(a) and (b). Apart from the nanohole orientations, we have kept the same geometric parameter value for both designs. The evanescent field generated at the analyte interface is crucial for exciting the SP resonance phenomenon, which is responsible for the sensing process on the analyte's interface. The strength of the field and sensitivity can be increased by optimizing the analyte's interaction with the field. The RI values for different materials used in our structure are listed in Table I.

Next, we have extracted the frequency response of both designs, follow Fig. 4. The position of the transmission peak depends upon several parameters, such as the elliptical

TABLE I
RI OF VARIOUS MATERIALS AT $\lambda = 633$ nm

Materials	Refractive Index (n+ik)
Silicon dioxide (SiO_2)	1.457
Air	1
Gold (Au)	0.18344+i3.4332
Sensing Material [26]	n_A=1.3739, n_B=1.3783, n_O=1.3778

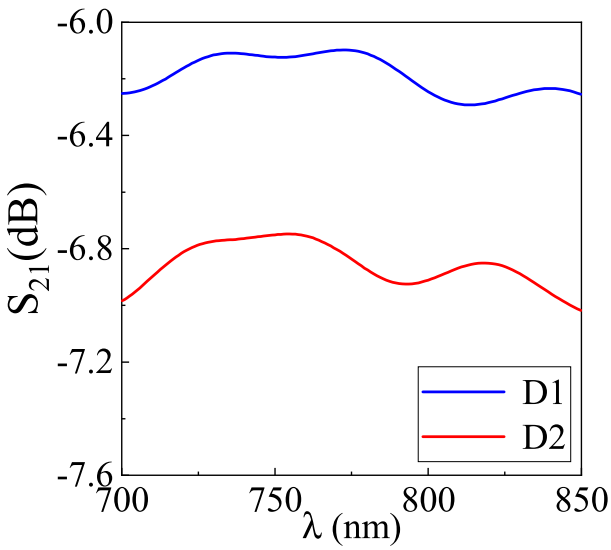

Fig. 4. Frequency response of Design 1 (solid blue) and Design 2 (solid red).

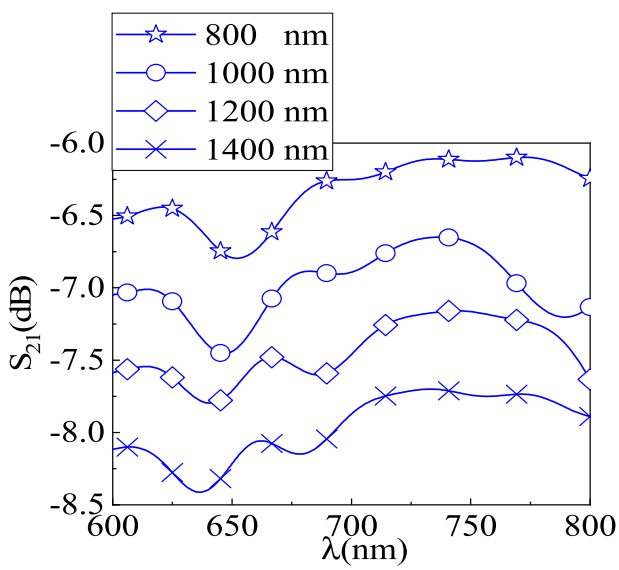

Fig. 5. Transmission spectrum of the MIM biosensor with different sensing regions' length (l).

nanohole's major and minor axis value, the sensing region's height and width, and the RI of both nanoholes and the surrounding medium. It can be observed that D1 has a higher transmission magnitude value in comparison with D2. The transmission of the elliptical-shaped hole array depends upon the orientation of the hole. The transmission magnitude value increases significantly when the major axis of the aperture is perpendicular to the polarization of the electric field [24].

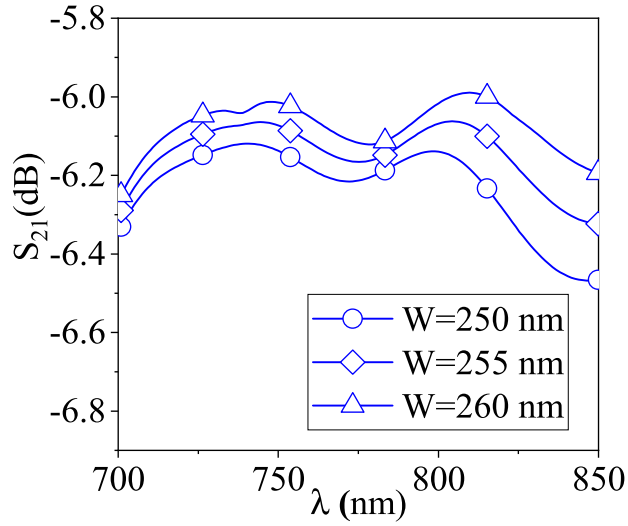

Fig. 6. Transmission plot of the proposed biosensor with different insulator widths (W).

TABLE II
OPTIMIZED DIMENSIONS OF THE PROPOSED BLOOD GROUP SENSOR

l	W	a_L	a_s	b_L	b_s
1000 nm	250 nm	50 nm	40 nm	30 nm	25 nm

The transmission spectrum with different sensing region lengths is plotted in Fig. 5. From Fig. 5; it can be observed that as the sensing region length increases, there is a significant decrease in the transmission of the proposed structure due to the increased ohmic metal losses.

The width of the sensing region has a great impact on the performance of the proposed sensor. The insulator width (W) is varied from 250 to 260 nm with an incremental step of 5 nm, while the other parameters of the sensors are kept constant, as plotted in Fig. 6. The increase in width of the sensing region leads to a corresponding increase in transmission parameters as well as shift the transmission peak toward a higher wavelength [27]. The height and width of the proposed structure are optimized using the finite element method-based COMSOL multiphysics software [22] and are also mentioned in Table II.

III. RESULTS AND DISCUSSION

The reported SPR-based biosensor can be used effectively for sensing several biological parameters, such as detecting pesticides, skin tissues, DNA, ribonucleic acid (RNA), and so on. We believe that our proposed sensor can be an ideal candidate for detecting any quantity that relies on the change of the RI. The proposed sensor can be used to identify the human blood group, as RI is an important characteristic of different types of blood groups. Based on the experimental results for the RI relation of three blood groups at the visible and near-infrared (NIR) wavelengths (360–860 nm), Li et al. [28] developed a Cauchy formula as written below:

$$n(\lambda)|_j = 1.357 + \frac{A_1}{\lambda^2} + \frac{A_2}{\lambda^4} \tag{4}$$

where λ is the wavelength (nm) and the subscript j = A, O, and B blood samples, respectively, Cauchy's coefficients A_1 and A_2 have a specific value for the three blood groups.

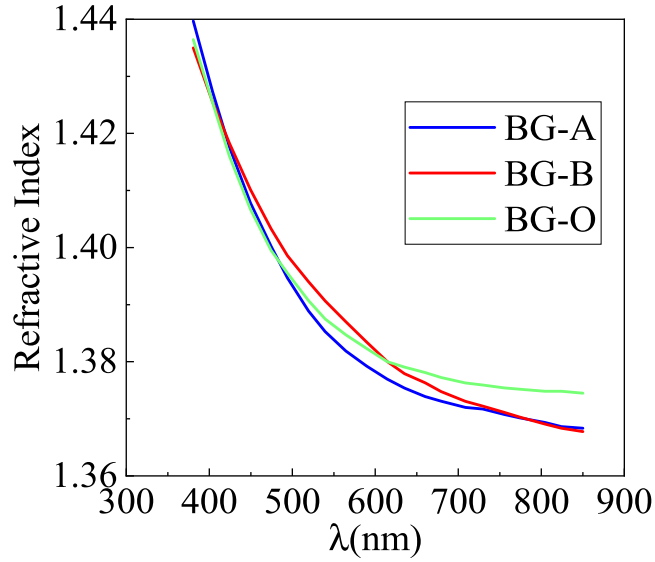

Fig. 7. RI versus wavelength variation for three different blood groups; solid blue: blood group A, solid red: Blood group B, and solid green: Blood group O.

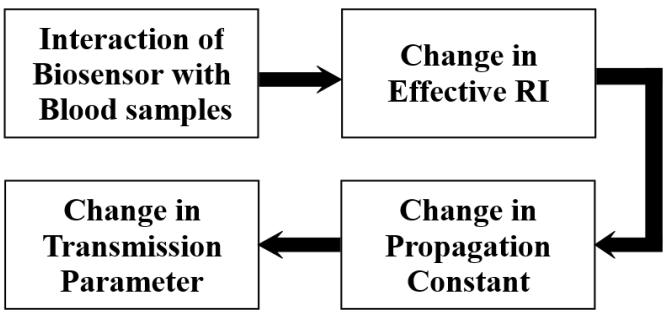

Fig. 8. Sensing principle of the suggested MIM biosensor.

The variation of RI with respect to wavelength is nonlinear in nature for three different blood groups (A, O, and B) (see Fig. 7). It can also be observed that there is a decrease in the RI value with the increase in the wavelength, which is the significant features of human blood groups. In addition to the wavelength, the RI of the blood group depends upon the hemoglobin concentration and the surrounding temperature. Hence, by taking into account the abovementioned parameters, the formula of the RI of the blood group, as discussed in (4), was modified to the following expression [30]:

$$n_{BG} = n_0 + \alpha D + \beta T + \gamma_1 \lambda + \gamma_2 \lambda^2 + \gamma_3 \lambda^3 \tag{5}$$

where D is the mass fraction of the dry hemoglobin (g/L), T represents the temperature (Kelvin), and λ denotes the wavelength (nm). α represents the concentration coefficient of RI of hemoglobin, and β represents the temperature coefficients of the RI. The variation in blood is reflected by several parameters, including the RI, hemoglobin concentration, temperature, and wavelength. The RI of different blood groups (O, A, and B) varies, and this changes the propagation constant (β_P) as per the relation given by $\beta_P = n_{BG} k_0$ (k_0 is the mode vector in a vacuum). As a result, the transmission parameter changes because it depends upon the propagation constant, which is represented by a block diagram, as shown in Fig. 8.

TABLE III
COEFFICIENTS OF (5) FOR DIFFERENT BLOOD GROUP SAMPLES [29]

Parameters	Units	O	B	A
n_0	-	1.54712	1.54712	1.54712
α	L/g	11.26×10^{-4}	11.09×10^{-4}	9.02×10^{-4}
D	g/L	108.9	111.1	146.2
β	1/°K	-6.5×10^{-5}	-6.5×10^{-5}	-6.5×10^{-5}
γ_1	1/nm	-8470×10^{-9}	-8470×10^{-9}	-8470×10^{-9}
γ_2	$1/nm^2$	774.2×10^{-9}	801.4×10^{-9}	708×10^{-9}
γ_3	$1/nm^3$	-0.182×10^{-9}	-0.228×10^{-9}	-0.128×10^{-9}

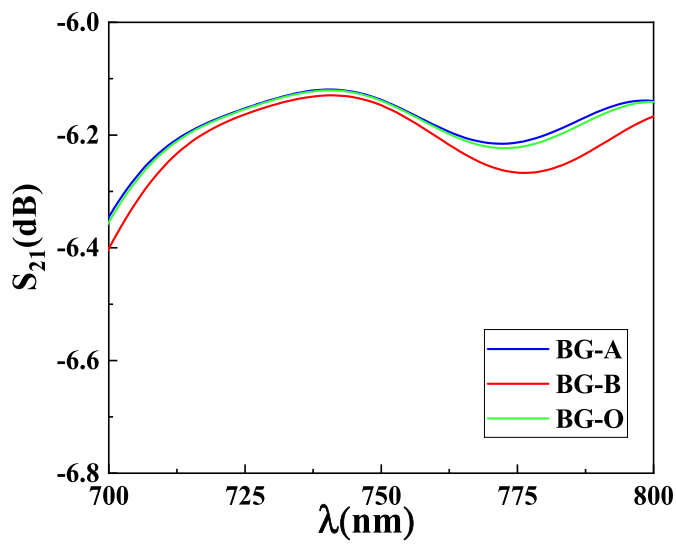

Fig. 9. Frequency response of MIM biosensor in the presence of different blood groups.

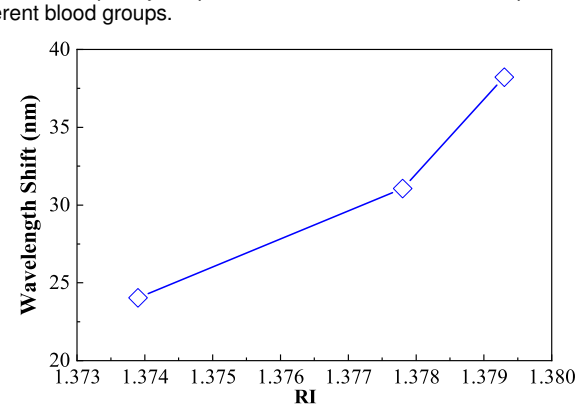

Fig. 10. Plot of wavelength shift versus RI.

The parameters used in our simulation to model RI of different blood groups are summarized in Table III. The transmission plot of various blood groups is shown in Fig. 9, where the blood samples are subjected to nanoholes.

Furthermore, Fig. 10 illustrates a plot representing the shift in wavelength as the RI changes from 1.373 to 1.380. It shows

TABLE IV
COMPARISON OF THE PROPOSED SENSOR WITH PREVIOUSLY REPORTED LITERATURE

Structure	Analyte/Sensing material	Sensitivity (*nm*/RIU)
Photonic crystal waveguide [32]	Blood	45.33
Photonic crystal fiber based on a ring resonator [33]	Blood	54.05
One-dimensional ternary photonic crystal waveguide with a defective layer [34]	Blood	51.49
One-dimensional photonic crystal-based biosensor [35]	Blood	75.00
This Work Metal-Insulator-Metal (MIM) waveguide	Blood	101.16

the behavior of resonance wavelength, specifically for the RI of the various blood groups, namely, A, O, and B. The suggested biosensor is capable of providing a resonance wavelength shift output for each incremental change of the RI.

This structure can be used as the blood group sensor by inserting the blood samples in the elliptical nanoholes, while the other parameters remain constant. Only a few drops of blood samples are enough for use in this structure as the sensing material because of the strong optical activity of plasmons in SPR sensors. The blood concentration, specifically the hemoglobin (*Hb*) concentration, plays a crucial role in determining the sensor parameters, such as DA and sensitivity of the sensor. There is a linear relationship between the hemoglobin concentration and the RI of the blood, as given in (5). Each blood group (O, A, and B) has a specific value of RI at a particular wavelength, as given in Table I. When the RI changes, there is a shift occurs in the transmission (alternatively, a shift occurs in the wavelength).

The sensor's performance is evaluated by a parameter known as sensitivity (S), defined as the ratio of change in wavelength ($\Delta\lambda$) to the change in RI (Δn) [24]. We have obtained three different sensitivity values for three different blood groups (A, O, and B): 64.26, 101.16, and 82.1 nm/RIU, respectively.

The DA of any sensor indicates the sharpness of the resonance dip and is defined as the reciprocal of the full-width at half-maximum (FWHM) [24]

$$\mathrm{DA} = \frac{1}{\mathrm{FWHM}}. \tag{6}$$

The smallest quantifiable change in RI of the proposed sensor is known as detection limit (DL), which is another crucial parameter of the performance of the plasmonic sensor,

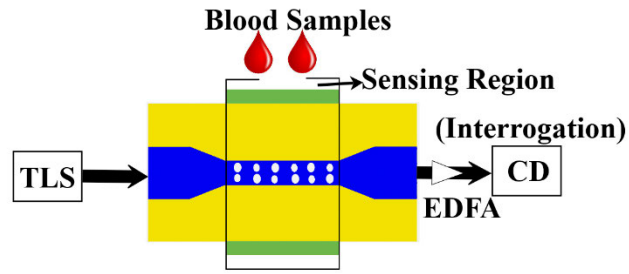

Fig. 11. Experimental setup for interrogation. Here, TLS—tunable laser source, EDFA—erbium-doped fiber amplifier, and CD—coherent detector.

and is defined by the following relation [31]:

$$\mathrm{DL} = \frac{\lambda_{\mathrm{FWHM}}}{20S} \tag{7}$$

where λ_{FWHM} denotes the FWHM of the transmission spectrum, and S denotes the sensor's sensitivity. We have calculated the abovementioned parameters of the proposed sensor, as shown in Fig. 1(a), by considering the length (l) and width (W) of the sensing region as 1000 and 250 nm, respectively. We have obtained the DA of 0.01 nm^{-1}, FoM of 1.02 RIU^{-1}, and DL of 0.05 RIU. The sensitivity value of our structure is compared with the sensitivity of the previously reported structure, as shown in Table IV. Additionally, we have shown a experimental setup in Fig. 11 to test its response in a real-world scenario.

IV. CONCLUSION

We have designed and theoretically studied a nanoscale MIM waveguide biosensor based on elliptical nanohole arrays to monitor the human blood group, namely, "A," "O," and "B." Its performance is enhanced with EOT via subwavelength nanoholes at the operating wavelength. The commercially available COMSOL multiphysics software optimizes the parameters of our proposed sensor. We have compared the two possible designs of the proposed sensor, and we have seen that design 1 ($D1$) achieves a sensitivity value of 64.26, 101.16, and 82.1 nm/RIU for three blood groups (A, O, and B), respectively. Therefore, the development and implementation of the proposed on-chip human blood group sensor represent a significant leap forward in the field of medical diagnostics and personalized medicine. The latest microfluidic technology and advanced human blood group detection methods help in safe blood transfusions, organ transplantation, and various medical treatments.

ACKNOWLEDGMENT

The authors would like to express their sincere thanks to the Department of Electronics and Communication Engineering at the National Institute of Technology Karnataka, Surathkal for providing research facilities and financial support for this research work.

REFERENCES

[1] H. Altug, S.-H. Oh, S. A. Maier, and J. Homola, "Advances and applications of nanophotonic biosensors," *Nature Nanotechnol.*, vol. 17, no. 1, pp. 5–16, Jan. 2022.

[2] H. Fu, S. Zhang, H. Chen, and J. Weng, "Graphene enhances the sensitivity of fiber-optic surface plasmon resonance biosensor," *IEEE Sensors J.*, vol. 15, no. 10, pp. 5478–5482, Oct. 2015.

[3] T. Dar, J. Homola, B. M. Azizur, and M. Rajarajan, "Label-free slot waveguide biosensor for the detection of DNA hybridization," *Appl. Opt.*, vol. 51, no. 34, pp. 8195–8202, Dec. 2012.

[4] S. K. Patel, J. Surve, J. Parmar, A. Natesan, and V. Katkar, "Graphene-based metasurface refractive index biosensor for hemoglobin detection: Machine learning assisted optimization," *IEEE Trans. Nanobiosci.*, vol. 22, no. 2, pp. 430–437, Apr. 2023.

[5] Z. Vafapour, "Polarization-independent perfect optical metamaterial absorber as a glucose sensor in food industry applications," *IEEE Trans. Nanobiosci.*, vol. 18, no. 4, pp. 622–627, Oct. 2019.

[6] P. Neutens, P. V. Dorpe, I. D. Vlaminck, L. Lagae, and G. Borghs, "Electrical detection of confined gap plasmons in metal–insulator–metal waveguides," *Nature Photon.*, vol. 3, pp. 283–286, May 2009.

[7] P. Berini, "Plasmon-polariton modes guided by a metal film of finite width bounded by different dielectrics," *Opt. Exp.*, vol. 7, no. 10, pp. 329–335, Nov. 2000.

[8] A. Dolatabady, N. Granpayeh, and V. F. Nezhad, "A nanoscale refractive index sensor in two dimensional plasmonic waveguide with nanodisk resonator," *Opt. Commun.*, vol. 300, pp. 265–268, Jul. 2013.

[9] S. Zhu and W. Zhou, "Plasmonic properties of two-dimensional metallic nanoholes fabricated by focused ion beam lithography," *J. Nanopart. Res.*, vol. 14, no. 3, p. 652, Feb. 2012.

[10] M. J. Al Mahmod, R. Hyder, and M. Z. Islam, "A highly sensitive metal–insulator–metal ring resonator-based nanophotonic structure for biosensing applications," *IEEE Sensors J.*, vol. 18, no. 16, pp. 6563–6568, Aug. 2018.

[11] M. Khodadadi, S. M. M. Moshiri, and N. Nozhat, "Theoretical analysis of a simultaneous graphene-based circular plasmonic refractive index and thickness bio-sensor," *IEEE Sensors J.*, vol. 20, no. 16, pp. 9114–9123, Aug. 2020.

[12] R. Zafar, S. Nawaz, G. Singh, A. D'Alessandro, and M. Salim, "Plasmonics-based refractive index sensor for detection of hemoglobin concentration," *IEEE Sensors J.*, vol. 18, no. 11, pp. 4372–4377, Jun. 2018.

[13] M. Sypabekova, A. Amantayeva, L. Vangelista, Á. González-Vila, C. Caucheteur, and D. Tosi, "Ultralow limit detection of soluble HER2 biomarker in serum with a fiber-optic ball-tip resonator assisted by a tilted FBG," *ACS Meas. Sci. Au*, vol. 2, no. 4, pp. 309–316, Mar. 2022.

[14] L. B. Melo et al., "Concentration sensor based on a tilted fiber Bragg grating for anions monitoring," *Opt. Fiber Technol.*, vol. 20, no. 4, pp. 422–427, Aug. 2014.

[15] M. S. Soares et al., "Label-free plasmonic immunosensor for cortisol detection in a D-shaped optical fiber," *Biomed. Opt. Exp.*, vol. 13, no. 6, pp. 3259–3274, Jun. 2022.

[16] R. A. M. Lameirinhas, J. P. N. Torres, A. Baptista, and M. J. M. Martins, "A new method to analyse the role of surface plasmon polaritons on dielectric-metal interfaces," *IEEE Photon. J.*, vol. 14, no. 4, pp. 1–9, Aug. 2022.

[17] M. Tavakoli, Y. S. Jalili, and S. M. Elahi, "Rayleigh-wood anomaly approximation with FDTD simulation of plasmonic gold nanohole array for determination of optimum extraordinary optical transmission characteristics," *Superlattices Microstruct.*, vol. 130, pp. 454–471, Jun. 2019.

[18] M. Tavakoli, Y. S. Jalili, and S. M. Elahi, "Phenomenological study of gold elliptical nanohole array as a plasmonic rotation sensor," *Opt. Commun.*, vol. 476, Dec. 2020, Art. no. 126336.

[19] S. K. Chamoli, S. C. Singh, and C. Guo, "Design of extremely sensitive refractive index sensors in infrared for blood glucose detection," *IEEE Sensors J.*, vol. 20, no. 9, pp. 4628–4634, May 2020.

[20] R. Jha and A. K. Sharma, "Design of a silicon-based plasmonic biosensor chip for human blood-group identification," *Sens. Actuators B, Chem.*, vol. 145, no. 1, pp. 200–204, Mar. 2010.

[21] J. A. Dionne, L. A. Sweatlock, H. A. Atwater, and A. Polman, "Plasmon slot waveguides: Towards chip-scale propagation with subwavelength-scale localization," *Phys. Rev. B, Condens. Matter*, vol. 73, no. 3, Jan. 2006, Art. no. 035407.

[22] *COMSOL Multiphysics Reference Manual*, COMSOL, Stockholm, Sweden, 2021.

[23] S. K. Sahu, S. K. Reddy, M. Singh, and E. Avrutin, "Hybrid plasmonic waveguide based platform for refractive index and temperature sensing," *IEEE Photon. Technol. Lett.*, vol. 34, no. 18, pp. 953–956, Sep. 15, 2022.

[24] A. K. Azad, Y. Zhao, and W. Zhang, "Transmission properties of terahertz pulses through an ultrathin subwavelength silicon hole array," *Appl. Phys. Lett.*, vol. 86, no. 14, Mar. 2005, Art. no. 141102.

[25] I. H. Malitson, "Interspecimen comparison of the refractive index of fused silica," *J. Opt. Soc. Amer.*, vol. 55, no. 10, pp. 1205–1208, 1965.

[26] P. S. Pandey, S. K. Raghuwanshi, R. Singh, and S. Kumar, "Surface plasmon resonance biosensor chip for human blood groups identification assisted with silver-chromium-hafnium oxide," *Magnetochemistry*, vol. 9, no. 1, pp. 1–11, Jan. 2023.

[27] S. H. Badri, "Transmission resonances in silicon subwavelength grating slot waveguide with functional host material for sensing applications," *Opt. Laser Technol.*, vol. 136, Apr. 2021, Art. no. 106776.

[28] H. Li, L. Lin, and S. Xie, "Refractive index of human whole blood with different types in the visible and near-infrared ranges," *Proc. SPIE*, vol. 3914, pp. 517–521, Jun. 2000.

[29] M. R. Rakhshani and M. A. Mansouri-Birjandi, "Engineering hexagonal array of nanoholes for high sensitivity biosensor and application for human blood group detection," *IEEE Trans. Nanotechnol.*, vol. 17, no. 3, pp. 475–481, May 2018.

[30] M. Yahya and M. Z. Saghir, "Empirical modelling to predict the refractive index of human blood," *Phys. Med. Biol.*, vol. 61, no. 4, pp. 1405–1415, Jan. 2016.

[31] Z. Chen, Y. Wang, Z. Hou, P. Zhang, and L. Yu, "Loaded slot cavity induced sensing enhancement and transparency based on plasmonic structure," *IEEE Sensors J.*, vol. 22, no. 14, pp. 14044–14050, Jul. 2022.

[32] H. Chopra, R. S. Kaler, and B. Painam, "Photonic crystal waveguide-based biosensor for detection of diseases," *J. Nanophotonics*, vol. 10, no. 3, Aug. 2016, Art. no. 036011.

[33] S. Singh and V. Kaur, "Photonic crystal fiber sensor based on sensing ring for different blood components: Design and analysis," in *Proc. 9th Int. Conf. Ubiquitous Future Netw. (ICUFN)*, Jul. 2017, pp. 399–403.

[34] H. J. El-Khozondar, P. Mahalakshmi, R. J. El-Khozondar, N. R. Ramanujam, I. S. Amiri, and P. Yupapin, "Design of one dimensional refractive index sensor using ternary photonic crystal waveguide for plasma blood samples applications," *Phys. E, Low-Dimensional Syst. Nanostruct.*, vol. 111, pp. 29–36, Jul. 2019.

[35] A. Bijalwan, B. K. Singh, and V. Rastogi, "Analysis of one-dimensional photonic crystal based sensor for detection of blood plasma and cancer cells," *Optik*, vol. 226, Jan. 2021, Art. no. 165994.

Santosh Kumar Sahu (Graduate Student Member, IEEE) received the B.Tech. degree in electronics and telecommunication engineering from the Indira Gandhi Institute of Technology Sarang, Odisha, India, in 2012, and the M.Tech. degree from the National Institute of Technology Silchar, Assam, India, in 2018. He is currently pursuing the Ph.D. degree in electronics and communication engineering with the National Institute of Technology Karnataka, Surathkal, India.

His current research interests include silicon photonics, hybrid plasmonic waveguides, and optical sensors.

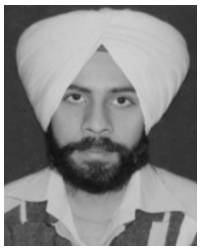

Mandeep Singh (Member, IEEE) received the M.Tech. degree from the IIT (ISM) Dhanbad, Jharkhand, India, in 2013, and the Ph.D. degree in electronics and communication engineering from the IIT Roorkee, Uttarakhand, India, in 2018.

He is working as an Assistant Professor with the Department of Electronics and Communication Engineering, National Institute of Technology Karnataka, Surathkal, India. He is also associated with the Department of ECE, Indian Institute of Science Bangalore, Bengaluru, India, as an INSA Visiting Scientist. His current research interests include silicon photonics, microwave photonics, and optical sensors.